Anomalous dynamic back-action in interferometers: beyond the scaling law

Sergey P. Tarabrin,[1, 2, *] Farid Ya. Khalili,[3] Henning Kaufer,[1] Roman Schnabel,[1] and Klemens Hammerer[1, 2]

[1]*Institut für Gravitationsphysik, Leibniz Universität Hannover and*
Max-Planck-Institut für Gravitationsphysik (Albert-Einstein-Institut), Callinstraße 38, 30167 Hannover, Germany
[2]*Institut für Theoretische Physik, Leibniz Universität Hannover, Appelstraße 2, 30167 Hannover, Germany*
[3]*Department of Physics, Moscow State University, Moscow 119992, Russia*
(Dated: December 27, 2012)

We analyze dynamic optomechanical back-action effects in signal-recycled Michelson and Michelson-Sagnac interferometers that are operated off dark port. Up to now, their optomechanics has been studied under dark port condition only. For the dark port case and in the context of gravitational wave detectors, the 'scaling law' assured that all back-action effects can be understood on the basis of the much simpler topology of a Fabry-Perot interferometer. Off dark port, our theoretical and experimental analysis reveals certain 'anomalous' features as compared to the ones of 'canonical' back-action, obtained within the scope of scaling law. In particular, optical damping as a function of detuning acquires a non-zero value on cavity resonance, and several stability/instability regions on either side of the cavity resonance appear. We report on the experimental observation of these instabilities on both sides of the cavity resonance in a Michelson-Sagnac interferometer with a micromechanical membrane. For a certain region of parameters, a stable optical spring (that is positive shifts of frequency *and* damping) in a free-mass interferometer with a single laser drive are possible. Our results can find implementations in both cavity optomechanics, revealing new regimes of cooling of micromechanical oscillators, and in gravitational-wave detectors, revealing the possibility of stable single-carrier optical spring which can be utilized for the reduction of quantum noise in future-generation detectors.

I. INTRODUCTION

It is a fundamental result of quantum measurement theory that in any optomechanical system, where light serves as the quantum readout agent interacting with a mechanical probe (test mass) via radiation pressure, the probe is subject to measurement *back-action* [1–3]. This comprises on the one hand *back-action noise*, that is radiation pressure noise on the test mass due to quantum fluctuations of the electromagnetic field. Together with measurement shot noise it gives rise to the celebrated standard quantum limit (SQL) of measurement precision [4–6]. The first observation of measurement back-action noise has been reported only very recently in Ref. [7]. On the other hand, modulation of the optical field by the motion of the probe (caused by any external forces) produces a ponderomotive radiation pressure force, which depends linearly on the displacement of the mechanical probe, and in turn alters the dynamical properties of the latter — this effect is referred to as *dynamic back-action*, and was first recognized in [8, 9] in the context of microwave cavities.

If the mechanical probe represents an oscillator, the dynamic back-action of light produces two effects: (i) optical rigidity (or optical spring) — a shift of the resonance frequency of the oscillator, and (ii) optical damping — a shift of the intrinsic damping rate of the oscillator. The experimental demonstration of the optical spring effect in a suspended Fabry-Perot cavity was reported in [10],

while optical damping was utilized in a series of recent experiments on back-action cooling [11, 12] of micromechanical oscillators [13–21], eventually to the quantum ground state [22, 23].

If the mechanical probe realizes a (quasi) free mass, as is the case of interferometric gravitational-wave detectors (GWDs), the dynamic back-action effectively transforms it into an oscillator whose rigidity and damping can have a rather complicated frequency dependence. In the context of GWDs this flexibility in tailoring the probe's dynamical properties was considered as a tool to increase the measurement sensitivity. In [24] the so-called intra-cavity readout GWD topology was suggested which utilized the optical rigidity. The sophisticated frequency dependence of the optical spring in the long Fabry-Perot cavities of GWDs was further analyzed in [25] and independently in [26]. Later on, it was shown that exactly the same frequency dependence arises in the dual-recycled topology of modern GWDs [27]. Ref. [28] derived the *scaling law* which provides a general framework for understanding dynamic back action in GWD topologies: it states that the dynamical and noise properties of any interferometer with high-finesse differential mode operated on a dark fringe (at dark port), are equivalent to the ones of a single Fabry-Perot cavity with corresponding effective linewidth, detuning and circulating optical power. In particular, the scaling law covers signal- and dual-recycled interferometers with or w/out arm cavities, and non-signal-recycled ones with arm-cavities. Based on this work, further studies of quantum-noise sensitivity of detuned-signal-recycling topology were performed [29, 30].

At the early stages of designing of the second-

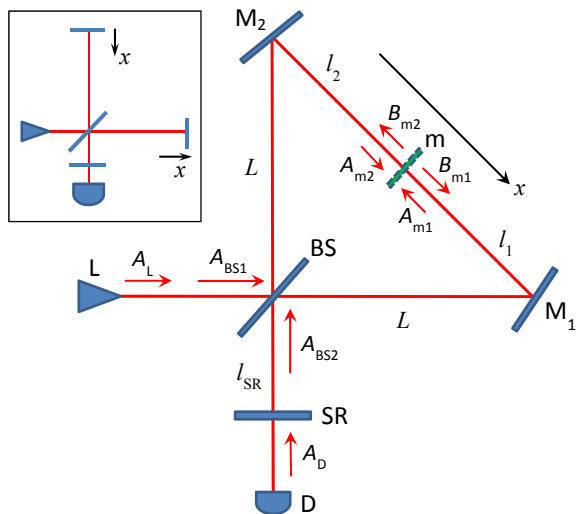*Corresponding author: Sergey.Tarabrin@aei.mpg.de

FIG. 1: Schematic of a signal-recycled Michelson-Sagnac interferometer as theoretically and experimentally investigated in this work. Inset: in the limiting case of 100% reflecting membrane Michelson-Sagnac interferometer is equivalent to a pure Michelson interferometer.

generation GWDs, like Advanced LIGO [31], the optical spring had been considered as the viable technology for suppression of quantum noises. Unfortunately, in the 'canonical' case of dark-port-tuned interferometers considered in Refs. [27, 28], the positive optical spring is always accompanied by a dynamical instability (negative damping). In Refs. [32, 33] it was shown theoretically and demonstrated experimentally that a stable configuration can be created by means of two optical carriers detuned to opposite sides of the interferometer resonance curve. Sensitivity issues of stable double-pumped optical spring were considered in Refs. [34, 35]. This idea was further developed into the concept of *negative optical inertia* [36], which also requires two oppositely detuned carriers and can be used for broadband suppression of quantum noise.

It became clear later on, however, that in the second-generation GWDs, due to sensitivity limitations imposed by the classical noise sources, in particular, coating Brownian noise of the test masses, only modest gain can be provided by the optical spring, which does not justify the accompanying technical difficulties (instability or the necessity to use two carriers). As a result, optical spring is currently not considered as an option for the second-generation GWDs [37]. The situation is different for the third-generation ones [38–40]. In these detectors classical noises will be reduced significantly (by implementing underground facilities, cryogenic cooling of the test masses, using low-loss and low-noise coatings, etc.), creating vast space for reduction of quantum noise. In this scenario, viable schemes for stable single-carrier optical inertia, as well as stable single-carrier optical spring are very desirable.

In this article we consider the dynamic back-action in a signal-recycled (SR) Michelson or Michelson-Sagnac (MS) interferometer, see Fig. 1, in a generic regime of operation *off dark port*. This is – to the best of the authors knowledge – the first analysis of back-action effects in interferometers operated in this mode. We emphasize that the generic way of performing a conventional, single photo-diode homodyne readout (DC readout) actually requires to tune the interferometer off dark fringe. Our analysis reveals certain 'anomalous' features of dynamic back-action, as compared to the ones of 'canonical' back-action, obtained within the scope of scaling law for interferometers operated on dark port. In particular, in the MS interferometer, given the finite reflectivity of the membrane, optical damping as a function of detuning acquires (i) non-zero value on resonance and (ii) *several* stability/instability regions on either side of the cavity resonance. We present experimental data on a signal-recycled MS interferometer containing a SiN membrane that, once operated off dark port, indeed exhibits two distinct instabilities on either side of the SR cavity resonance. In the case of a perfectly reflecting membrane, which corresponds to a simple Michelson interferometer, the off-dark-port regime similarly results in several intersecting regions of positive/negative values of optical rigidity and damping. For a certain region of parameters, stable sets of both effects in a free-mass interferometer with a single laser drive are possible. Our results can find applications in both cavity optomechanics, revealing new regimes of cooling of micromechanical oscillators, and in the gravitational-wave detectors, revealing the possibility of stable single-carrier optical spring which can be utilized for the reduction of quantum noise in future-generation detectors.

Our results for generic signal-recycled Michelson and MS interferometers are related to and consistent with corresponding findings for high-finesse optomechanical cavities exhibiting a so-called *dissipative* (or *reactive*) optomechanical coupling. In this case, mechanical displacement shifts the line width of the cavity, and not its resonance frequency, which gives rise to Fano resonances in the back-action noise spectrum, as was shown in [41]. Traces of such a coupling have been observed in [42]. Several theoretical studies explored the rich implications of this coupling on position sensing and mechanical squeezing [41, 43], normal mode splitting and multiple regions of instability [44, 45]. Some of the authors showed recently that a *pure* dissipative optomechanics can in fact be achieved in a MS interferometer with a semitransparent micromechanical membrane [46]. As we show here, the feature of Fano resonances in back-action noise, and associated anomalous effects in damping and rigidity, have to be expected as a generic property of Michelson and MS interferometers operated off dark port.

This paper in organized as follows. In the first part (Sec. II) we compare 'canonical' dynamic back-action, derived within the scope of scaling law, to the 'anomalous' one which is rigorously derived in the second part. We apply the transfer matrix approach to the propagation of

fields inside the interferometer (Sec. III), in the spirit of Ref. [3]. We compute optical fields on the membrane surfaces and corresponding radiation pressure force, which is the sum of a stochastic part (back-action noise, Sec. IV) and a dynamical part (dynamic back-action, Sec. V). In Sec. VI we report on the experimental observation of instabilities on both sides of the cavity resonance in a Michelson-Sagnac interferometer with a micromechanical membrane. Finally, we analyze certain properties of the obtained quantities and draw conclusions.

II. CANONICAL AND ANOMALOUS DYNAMIC BACK-ACTION

The dynamic back-action $\mathcal{K}(\Omega)$ is defined as the coefficient of proportionality between the ponderomotive radiation pressure force $F_x(\Omega)$ and displacement of the mechanical probe $x(\Omega)$, $F_x(\Omega) = -\mathcal{K}(\Omega)x(\Omega)$. It comprises the optical spring $K(\Omega) = \Re[\mathcal{K}(\Omega)]$ and optical damping $\Gamma(\Omega) = -\frac{1}{2}\Im[\mathcal{K}(\Omega)]/\Omega$, such that the corresponding shifts of the (square of) mechanical frequency and mechanical damping rate are K/m and Γ/m, with m being the oscillator's mass. So far, the dynamic back-action has been studied in the literature only for interferometers perfectly tuned to dark port. According to the scaling law [28], any interferometer with high-finesse differential mode and operated at dark port, can be equivalently described by a single Fabry-Perot cavity with effective half-linewidth γ, detuning Δ and circulating optical power P_{cav}. Thus, the optical spring and damping in an interferometer reduce in this case to the well-known ones of a FP cavity [25],

$$K(\Omega) = \frac{2\omega_0\mathcal{E}}{L^2}\frac{\Delta(\Delta^2 + \gamma^2 - \Omega^2)}{|\Delta^2 + (\gamma - i\Omega)^2|^2}, \qquad (1a)$$

$$\Gamma(\Omega) = -\frac{2\omega_0\mathcal{E}}{L^2}\frac{\Delta\gamma}{|\Delta^2 + (\gamma - i\Omega)^2|^2}, \qquad (1b)$$

where ω_0 is laser carrier frequency, $\mathcal{E} = 2LP_{\mathrm{cav}}/c$ is the optical energy stored inside the cavity and L is cavity length. These 'canonical' rigidity and damping posses the following characteristic features: (i) both are antisymmetric with respect to Δ and vanish at $\Delta = 0$, (ii) Γ as a function of Δ crosses zero only once, thus being positive for $\Delta < 0$ and negative for $\Delta > 0$ — these regions are usually labeled as stable (cooling) and unstable (heating), (iii) K as a function of Δ crosses zero once if $\gamma \geq \Omega$ (case of free-mass interferometers) and (iv) three times otherwise (case of micromechanical oscillators in the resolved sideband limit). These properties are illustrated in Fig. 2a. In a Hamiltonian formulation of cavity optomechanics Eqs. (1a, 1b) follow from $H_{\mathrm{int}} = g_\omega x a^\dagger a$, with g_ω being the coupling constant between intracavity field a and position of the mechanical oscillator x [2]. This is usually addressed as dispersive coupling, since the mechanical oscillations modulate the cavity eigenfrequencies.
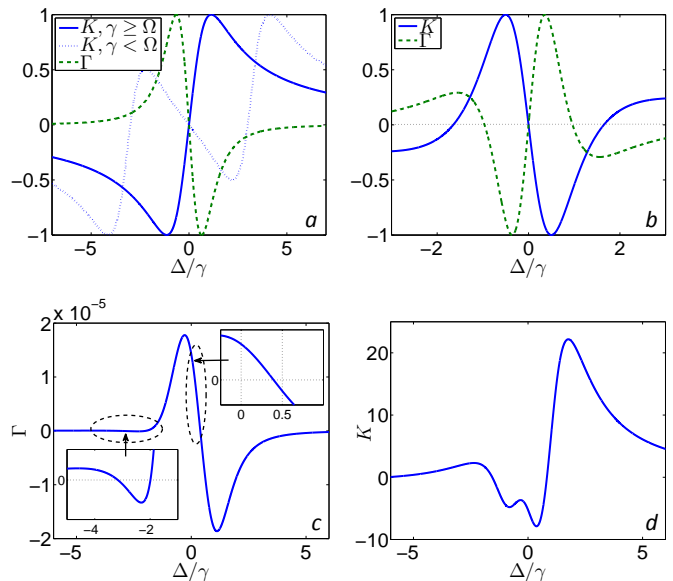

FIG. 2: Optical spring K and optical damping Γ as functions of detuning (in units of cavity half-linewidth γ). Curves are plotted for the following parameters: membrane power reflectivity $R_{\mathrm{m}}^2 = 0.17$ (except b), SRM transmittance $T_{\mathrm{SR}}^2 = 3 \times 10^{-4}$, beamsplitter asymmetry $\delta_{\mathrm{BS}} = 0$. a. Normalized to maximum values 'canonical' K and Γ defined in Eqs. (1a, 1b). b. Normalized to maximum values K and Γ for the MS interferometer with 100%-reflective membrane (equivalently, a pure Michelson interferometer), detuned from dark port at $\delta l_{\mathrm{DP}} = \lambda_0/4$ by $\delta l - \delta l_{\mathrm{DP}} \approx 0.01\lambda_0$. Ratio of the mechanical frequency to cavity linewidth is $\Omega/\gamma \approx 10^{-2}$. Optical damping ($c$) and spring ($d$) for a MS interferometer detuned from dark port at $\delta l_{\mathrm{DP}} = 3\lambda_0/4$ by $\delta l - \delta l_{\mathrm{DP}} \approx 0.01\lambda_0$, input optical power $P_{\mathrm{in}} = 200$ mW, laser carrier wavelength $\lambda_0 = 1064$ nm, effective cavity length $\mathcal{L} = 8.7$ cm and $\Omega/\gamma \approx 1$.

Our analysis in Sec. V shows that in a signal-recycled MS interferometer these features expectedly hold in dark port, but if detuned from it, features (i) — (iii) break. In this sense we refer to the dynamic back-action in a MS interferometer operated off dark fringe as 'anomalous'. In particular, both K and Γ become highly asymmetric and acquire non-zero values at $\Delta = 0$ (see Fig. 2c,d), so that for certain region of parameters $\Gamma|_{\Delta=0} > 0$ — this is *cooling on resonance* (see upper inset in Fig. 2c). Also optical damping can cross zero several times, acquiring additional regions of stability/instability (see lower inset in Fig. 2c), thus allowing *another regime of cooling*. In Sec. VI we report on the experimental observation of these instabilities on both sides of the cavity resonance in a Michelson-Sagnac interferometer with a micromechanical membrane. Non-zero K at $\Delta = 0$ implies a shift of the mechanical frequency on resonance, though for micromechanical oscillators it is mostly negligible compared to intrinsic mechanical frequencies.

An extreme case of a 100% reflective membrane corresponds to a pure Michelson interferometer, i.e. repro-

duces basic topology of the GW detectors. The coordinate x of the mechanical degree of freedom refers then to the differential motion of the end-mirrors in the arms of the Michelson interferometer, cf. Fig. 1. For a GW detector being a free-mass interferometer the effect of optical spring is not negligible, since it transforms (almost) free test masses into mechanical oscillators with resonance frequencies lying in the GW observation band, where typically $\Omega < \gamma$. Thus, if a detuned interferometer is operated at dark fringe, Eqs. (1a, 1b) imply either $K > 0, \Gamma < 0$ for $\Delta > 0$, or $K < 0, \Gamma > 0$ for $\Delta < 0$. This means that for a single laser drive a set of 'canonical' K and Γ is unstable in both cases.

It is rather intriguing, however, that the well-studied Michelson interferometer also exhibits 'anomalous' dynamic back-action if operated off dark port, violating features (ii) and (iii) of the 'canonical' one: according to Eq. (13), two regions of positive/negative values can arise in both K and Γ, as illustrated in Fig. 2b. For a GW detector this opens up a region of parameters where sets of K and Γ result in *a stable configuration for a single laser drive.* Indeed, one can notice in Fig. 2b a ceratin range of negative detunings where both optical spring and damping are positive, indicating a possible stable state, which is confirmed by the accurate analysis of stability in terms of Routh-Hurwitz criteria. Moreover, an 'anomalous' optical spring (not necessary stable) can naturally occur in any detuned interferometer with a DC-readout (like AdvLIGO or GEO-HF [47]) when an offset from dark fringe is created on purpose to get a small fraction of mean power for the homodyne detection.

Ref. [46] considered a MS interferometer with 100% reflective recycling mirror in a general regime of operation. In an effective-cavity approach (valid for a high-finesse signal recycling cavity) it was shown there that the system can be described by a Hamiltonian $H_{\text{int}} = g_\omega(x)a^\dagger a + g_\gamma(x) \int d\omega(a_\omega^\dagger a - \text{h.c.})$. The last term describes coupling of the cavity field a to the continuum of modes a_ω of the in/out-going external field, which will cause an amplitude decay (linewidth) $\propto g_\gamma^2$. In this system, the mechanical oscillator modulates both, the cavity resonance (via g_ω) *and* the cavity linewidth (via g_γ). These two aspects are referred to as dispersive and dissipative coupling [41, 45], respectively. Therefore, in a regime where an effective cavity description is adequate, deviations from Eqs. (1a, 1b) can be explained by the emergence of dissipative coupling in addition to the dispersive one and interplay between them. However, in interferometers where such a description is not valid these labels cannot be unambiguously attributed. We therefore shall further talk of the interferometers operated at or off dark fringe as demonstrating 'canonical' or 'anomalous' dynamical back-action. 'Anomalous' back-action in this sense is the generalization of the 'canonical' one, which corresponds to the particular case of dark-port-tuned interferometers, and thus violates the scaling law.

III. PROPAGATION OF FIELDS

Consider a Michelson-Sagnac interferometer as shown in Fig. 1 with a central beamsplitter BS having amplitude reflectivity $R_{\text{BS}} = \sqrt{(1 - \delta_{\text{BS}})/2}$ and transmissivity $T_{\text{BS}} = \sqrt{(1 + \delta_{\text{BS}})/2}$, two steering mirrors M_1 and M_2 both having 100% reflectivity, a semitransparent membrane m with amplitude reflectivity R_{m} and transmissivity T_{m}, and a signal-recycling mirror SR with amplitude reflectivity R_{SR} and transmissivity T_{SR}. The interferometer is driven by a laser L through laser port which is usually labeled as 'bright port'. Photons emanating through the other, detector (or 'dark') port impinge on a detector D (homodyne or heterodyne). Note that if the offset from dark fringe is large enough, traditional labels 'bright' and 'dark' port become ambiguous. Unless mentioned explicitly, we neglect losses. We denote the distance between SR mirror and BS as l_{SR}, arm length as L and the distances between folding mirrors M_1 and M_2 and membrane as $l_1 = l - \delta l/2$ and $l_2 = l + \delta l/2$, respectively. This means that $l_1 + l_2 = 2l$, $l_2 - l_1 = \delta l$ and the mean position of the membrane on the x-axis is $\langle x \rangle = \delta l/2$. The total length of the SR-m path is $\mathcal{L} = L + l + l_{\text{SR}}$.

In any spatial location inside the interferometer we decompose the electric field of the coherent, plane and linearly polarized electromagnetic wave into the sum of a steady-state (mean) field with amplitude A_0 and carrier frequency ω_0 (wavenumber $k_0 = \omega_0/c$ and wavelength $\lambda_0 = 2\pi/k_0$), and slowly-varying (on the scale of $1/\omega_0$) perturbation field with amplitude $a(t)$ describing vacuum noises and the contribution from the motion of the membrane,

$$A(t) = \sqrt{\frac{2\pi\hbar\omega_0}{\mathcal{A}c}} \left[A_0 e^{-i\omega_0 t} + a(t)e^{-i\omega_0 t} \right] + \text{h.c.},$$

$$a(t) = \int_{-\infty}^{+\infty} a(\omega_0 + \Omega)e^{-i\Omega t} \frac{d\Omega}{2\pi}.$$

Here $\mathcal{A}$ is the area of laser beam's cross-section and c is the speed of light. Unless mentioned explicitly, we will deal with fields in the frequency domain only. We will therefore omit frequency arguments for briefness.

The laser L emits a drive-wave A_{L} with mean amplitude A_{L0} and optical fluctuations a_{L}. For simplicity we assume that there are no technical fluctuations so that the laser is shot-noise limited, $[a_{\text{L}}(\omega_0 + \Omega), a_{\text{L}}^\dagger(\omega_0 + \Omega')] = 2\pi\delta(\Omega - \Omega')$. The vacuum field A_{D} entering through the SR mirror (SRM) from detector port has zero mean amplitude but non-zero vacuum noise a_{D}, uncorrelated with vacuum noise from the laser port and obeying the similar commutation relation $[a_{\text{D}}(\omega_0 + \Omega), a_{\text{D}}^\dagger(\omega_0 + \Omega')] = 2\pi\delta(\Omega - \Omega')$. We unite these into vector-column of input fields $\boldsymbol{A}_{\text{in}} = (A_{\text{L}}, A_{\text{D}})$, so that the vector of mean input fields is $\boldsymbol{A}_{\text{in0}} = (A_{\text{L0}}, 0)$ and the vector of perturbation fields is $\boldsymbol{a}_{\text{in}} = (a_{\text{L}}, a_{\text{D}})$. Due to linearity of the system input fields can be propagated throughout the interferometer as independent Fourier components.

Consider first the case without SRM and with a fixed membrane. The latter condition allows us to treat mean and perturbation fields on equal footing. Input fields (in this case coinciding with the fields incident on the beamsplitter) linearly transform into the output fields: first they split/combine on the beamsplitter, travel along distances L in both arms, reflect from the steering mirrors, travel distances $l_{1,2}$ towards the membrane, reflect/transmit on it, then travel backwards distances $l_{1,2}$ and L and finally recombine at the beamsplitter. Each transformation is defined by the corresponding transfer matrix and the round-trip of light is defined by their product, $\boldsymbol{A}_{\text{out}} = \mathbb{M}_{\text{BS}}^T \mathbb{P}_L \mathbb{P}_l \mathbb{M}_{\text{m}} \mathbb{P}_l \mathbb{P}_L \mathbb{M}_{\text{BS}} \boldsymbol{A}_{\text{in}} \equiv \mathbb{M}_{\text{MS}} \boldsymbol{A}_{\text{in}}$. Here

$$\mathbb{M}_{\text{BS}} = \begin{pmatrix} T_{\text{BS}} & -R_{\text{BS}} \\ R_{\text{BS}} & T_{\text{BS}} \end{pmatrix}, \quad \mathbb{M}_{\text{m}} = \begin{pmatrix} -R_{\text{m}} & T_{\text{m}} \\ T_{\text{m}} & R_{\text{m}} \end{pmatrix}, \quad (2)$$

are the transformation matrices of beamsplitter and membrane, both chosen in real form (this is always possible due to Stokes relations), and

$$\mathbb{P}_L = \begin{pmatrix} e^{ikL} & 0 \\ 0 & e^{ikL} \end{pmatrix}, \quad \mathbb{P}_l = \begin{pmatrix} e^{ikl_1} & 0 \\ 0 & e^{ikl_2} \end{pmatrix},$$

are the propagation matrices comprised of the phase shifts along the horizontal/vertical arms (of length L) and diagonal half-arms (of lengths $l_{1,2}$). For mean fields one should apply the substitution $k = k_0$ and for perturbation fields $k = k_0 + K = k_0 + \Omega/c$. The matrix $\mathbb{M}_{\text{MS}}$ thus represents the transformation matrix of a non-recycled Michelson-Sagnac interferometer

$$\mathbb{M}_{\text{MS}} = e^{2ik(L+l)} \begin{pmatrix} \rho_1 & \tau \\ \tau & \rho_2 \end{pmatrix},$$

with

$$\begin{aligned}
\rho_1 &= R_{\text{m}} \left(R_{\text{BS}}^2 e^{ik\delta l} - T_{\text{BS}}^2 e^{-ik\delta l} \right) + 2 T_{\text{m}} R_{\text{BS}} T_{\text{BS}}, \\
\rho_2 &= R_{\text{m}} \left(T_{\text{BS}}^2 e^{ik\delta l} - R_{\text{BS}}^2 e^{-ik\delta l} \right) - 2 T_{\text{m}} R_{\text{BS}} T_{\text{BS}}, \\
\tau &= R_{\text{m}} R_{\text{BS}} T_{\text{BS}} \left(e^{ik\delta l} + e^{-ik\delta l} \right) + T_{\text{m}} (T_{\text{BS}}^2 - R_{\text{BS}}^2).
\end{aligned}$$

Physically ρ_1 is the reflectivity of the input laser field back into the laser port, $\rho_2 = -\rho_1^*$ is the reflectivity of input vacuum field back into detector port, and τ is the transmissivity of the laser field into detector port and vacuum field into laser port. One can check that the matrix $\mathbb{M}_{\text{MS}}$ is unitary, thus *non-recycled MS interferometer can be described as an effective mirror with reflectivity and transmissivity depending on membrane position* via δl. The dark port (dark fringe) condition for the interferometer is achieved when the cross-transmittance between input-output ports vanishes (in particular, no mean power leaks into the detector port), corresponding to $\tau = 0$, or explicitly

$$\cos k_0 \delta l = -\frac{T_{\text{m}}}{R_{\text{m}}} \frac{\delta_{\text{BS}}}{\sqrt{1 - \delta_{\text{BS}}^2}}. \quad (3)$$

In the case of a symmetric beamsplitter ($\delta_{\text{BS}} = 0$) this is satisfied for $\delta l = n\lambda_0/4$ and odd n [56].

If the SRM is inserted then the out-going field in the SR port is reflected back, such that the in-going fields incident on the beamsplitter are defined by the equation

$$\boldsymbol{A}_{\text{BS}} = \mathbb{P}_R \mathbb{T}_R \boldsymbol{A}_{\text{in}} + \mathbb{P}_R \mathbb{R}_R \mathbb{P}_R \mathbb{M}_{\text{MS}} \boldsymbol{A}_{\text{BS}}. \quad (4)$$

Here $\boldsymbol{A}_{\text{BS}} = (A_{\text{BS1}}, A_{\text{BS2}})$ is the vector-column of in-going beamsplitter fields (see Fig. 1), $\mathbb{R}_R = \text{diag}(0, R_{\text{SR}})$ with zero standing for the absence of power-recycling mirror in laser port, $\mathbb{P}_R = \text{diag}(1, e^{ikl_{\text{SR}}})$ is the propagation matrix in BS-SR path, and $\mathbb{T}_R = \text{diag}(1, T_{\text{SR}})$. Thus the first summand on the RHS of Eq. (4) stands for the input fields directly incident on the beamsplitter, while the second summand corresponds to a single round trip along the interferometer with reflection from the SRM. Solution of this equation yields

$$\boldsymbol{A}_{\text{BS}} = (\mathbb{I} - \mathbb{P}_R \mathbb{R}_R \mathbb{P}_R \mathbb{M}_{\text{MS}})^{-1} \mathbb{P}_R \mathbb{T}_R \boldsymbol{A}_{\text{in}}, \quad (5)$$

where $\mathbb{I}$ is the 2×2 unity matrix. Denote inverse matrix in this solution as $\mathbb{K}_{\text{MSR}}$,

$$\mathbb{K}_{\text{MSR}} = \frac{1}{\mathcal{D}} \begin{pmatrix} \mathcal{D} & 0 \\ R_{\text{SR}} \tau e^{2ik\mathcal{L}} & 1 \end{pmatrix}, \quad \mathcal{D} = 1 - R_{\text{SR}} \rho_2 e^{2ik\mathcal{L}}.$$

This tells us that *the MS interferometer with SR mirror makes an effective Fabry-Perot cavity* with associated resonance factor $1/\mathcal{D}$. The matrix element $\mathbb{K}_{\text{MSR}}^{(2,2)}$ describes a resonant amplification of input vacuum field inside the cavity, while $\mathbb{K}_{\text{MSR}}^{(2,1)}$ corresponds to the laser field being partially transmitted into the SR port (hence the proportionality to τ) and also enhanced inside the cavity. In the ideal dark-port regime cross-transmittance is suppressed, all laser field is reflected back into laser port, and only the vacuum field from the detector port resonates inside the cavity.

Note that the effective detuning of the laser carrier from cavity resonance(s) is not solely defined by the corresponding shift in frequnecy (or cavity length) in contrast to the ordinary Fabry-Perot cavity. Assume that $k\mathcal{L} = \pi N + \delta_k \mathcal{L}$, N is integer, $\delta_k \mathcal{L} \ll 1$, and $\arg \rho_2 = \phi_{\text{DP}} + \delta\phi$, where $\phi_{\text{DP}} = \arg \rho_2|_{\text{dark port}}$ and $\delta\phi$ is the deviation from it due to offset from dark fringe via membrane positioning. Then one can rewrite the inverse resonance factor as

$$\mathcal{D} = 1 - R_{\text{SR}} |\rho_2| e^{2i\delta_k \mathcal{L} + i \arg \rho_2} = 1 - R_{\text{SR}} |\rho_2| e^{2i\Delta_k \mathcal{L}},$$

such that the full detuning

$$\Delta_k = \left(\delta_k + \frac{\phi_{\text{DP}}}{2\mathcal{L}} \right) + \frac{\delta\phi}{2\mathcal{L}} = \delta_k' + \frac{\delta\phi}{2\mathcal{L}}, \quad (6)$$

is the sum of the 'conventional' detuning $\delta = c\delta_k'$ of carrier frequency from cavity resonance at dark port, and an additional detuning $\delta\phi/(2\mathcal{L})$ corresponding to the offset from the latter.

The narrow-band limit is achieved when both SR mirror and compound 'interferometer' mirror possess high

reflectivity, $1 - R_{\text{SR}} \approx T_{\text{SR}}^2/2 \ll 1$ and $1 - |\rho_2| \approx \tau^2/2 \ll 1$. The half-linewidth of the cavity is then

$$\gamma = \frac{1 - R_{\text{SR}}|\rho_2|}{2\mathcal{L}/c} \approx \frac{cT_{\text{SR}}^2}{4\mathcal{L}} + \frac{c\tau^2}{4\mathcal{L}}. \tag{7}$$

Therefore, the total cavity linewidth accounts for finite SRM transmittance and finite transmittance of the interferometer operated off dark port; since $\tau = \tau(\delta l)$, the latter contribution describes modulation of the linewidth by the motion of the membrane, thus implementing dissipative coupling, as discussed already in [46]. If the optical losses in the system are symmetric with respect to interferometer arms, then one can add the corresponding loss factor to T_{SR}^2, since it is the SRM that couples vacuum noise into the interferometer. Otherwise, one can take asymmetric losses into account, for example, by assigning finite transmittances to the steering mirrors $M_{1,2}$ and taking into account vacuum noises entering through them.

IV. STOCHASTIC BACK-ACTION

In order to determine the radiation pressure force acting on the membrane we need to determine the fields on the membrane surfaces. In-going fields on the beamsplitter (5) propagate along the arms and transform into the fields incident on the membrane $(A_{\text{m}1}, A_{\text{m}2}) = \boldsymbol{A}_{\text{m}} = \mathbb{P}_l \mathbb{P}_L \mathbb{M}_{\text{BS}} \boldsymbol{A}_{\text{BS}}$ and reflected from it $(B_{\text{m}1}, B_{\text{m}2}) = \boldsymbol{B}_{\text{m}} = \mathbb{M}_{\text{m}} \boldsymbol{A}_{\text{m}}$, see Fig. 1. In terms of input fields

$$\boldsymbol{A}_{\text{m}} = \mathbb{M}_A \boldsymbol{A}_{\text{in}}; \quad \mathbb{M}_A = \mathbb{P}_l \mathbb{P}_L \mathbb{M}_{\text{BS}} \mathbb{K}_{\text{MSR}} \mathbb{P}_R \mathbb{T}_R, \tag{8a}$$

$$\boldsymbol{B}_{\text{m}} = \mathbb{M}_B \boldsymbol{A}_{\text{in}}; \quad \mathbb{M}_B = \mathbb{M}_{\text{m}} \mathbb{P}_l \mathbb{P}_L \mathbb{M}_{\text{BS}} \mathbb{K}_{\text{MSR}} \mathbb{P}_R \mathbb{T}_R. \tag{8b}$$

The components of matrices $\mathbb{M}_A$ and $\mathbb{M}_B$ are presented in the Appendix. Denote these transfer matrices separately for mean fields as $\mathbb{M}_{A_0} = \mathbb{M}_A|_{k=k_0}$, $\mathbb{M}_{B_0} = \mathbb{M}_B|_{k=k_0}$ and perturbation fields as $\mathbb{M}_a(\Omega) = \mathbb{M}_A|_{k=k_0+K}$, $\mathbb{M}_b(\Omega) = \mathbb{M}_B|_{k=k_0+K}$.

The radiation pressure force exerted on the membrane is then given by

$$F(t) = -\frac{\mathcal{A}}{4\pi} \left\langle A_{\text{m}1}^2(t) + B_{\text{m}1}^2(t) - A_{\text{m}2}^2(t) - B_{\text{m}2}^2(t) \right\rangle, \tag{9}$$

where averaging is performed over the period of electromagnetic oscillations. Ignoring the D.C. contribution and linearizing with respect to perturbation terms, the spectrum of the force reads

$$F_{\text{BA}}(\Omega) = 2\hbar k_0 R_{\text{m}} \boldsymbol{A}_{\text{in}0}^{*T} \mathbb{M}_{A_0}^{*T} \mathbb{M}_b(\Omega) \boldsymbol{a}_{\text{in}}(\omega_0 + \Omega)$$
$$+ 2\hbar k_0 R_{\text{m}} \boldsymbol{A}_{\text{in}0}^{T} \mathbb{M}_{A_0}^{T} \mathbb{M}_b^*(-\Omega) \boldsymbol{a}_{\text{in}}^{\dagger}(\omega_0 - \Omega).$$

This is the radiation pressure noise, also addressed as back-action noise or stochastic back-action, i.e. the time-varying radiation pressure that is solely caused by the fluctuations of optical fields. The unsymmetrized spectral density of stationary back-action noise

is computed from the equation $2\pi\delta(\Omega - \Omega')S_F(\Omega') = \langle 0|F_{\text{BA}}(\Omega)F_{\text{BA}}^{\dagger}(\Omega')|0\rangle$, yielding

$$S_F(\Omega) = \frac{4\hbar k_0}{c} \frac{R_{\text{m}}^2 P_{\text{in}}}{|\mathcal{D}_0 \mathcal{D}(\Omega)|^2} \left\{ |\mathfrak{L}(\Omega)|^2 + T_{\text{SR}}^2 |\mathfrak{D}(\Omega)|^2 \right\}, \tag{10}$$

$$\mathfrak{L}(\Omega) = \alpha_1 \left(1 + R_{\text{SR}}^2 e^{2iK\mathcal{L}}\right) + \alpha_2 R_{\text{SR}} e^{2i(k_0+K)\mathcal{L}}$$
$$+ \alpha_2^* R_{\text{SR}} e^{-2ik_0\mathcal{L}},$$
$$\mathfrak{D}(\Omega) = \beta_1 + \beta_2 R_{\text{SR}} e^{-2ik_0\mathcal{L}},$$
$$\alpha_1 = T_{\text{m}} R_{\text{BS}} T_{\text{BS}} \left(e^{ik\delta l} + e^{-ik\delta l}\right) - R_{\text{m}}(T_{\text{BS}}^2 - R_{\text{BS}}^2),$$
$$\alpha_2 = T_{\text{BS}}^2 e^{ik\delta l} + R_{\text{BS}}^2 e^{-ik\delta l},$$
$$\beta_1 = T_{\text{m}} \left(T_{\text{BS}}^2 e^{ik\delta l} - R_{\text{BS}}^2 e^{-ik\delta l}\right) + 2R_{\text{m}} R_{\text{BS}} T_{\text{BS}},$$
$$\beta_2 = R_{\text{BS}} T_{\text{BS}} \left(e^{ik\delta l} - e^{-ik\delta l}\right).$$

Here $P_{\text{in}} = \hbar\omega_0 |A_{\text{L}0}|^2$ is the input laser power, $\mathcal{D}_0 = \mathcal{D}|_{k=k_0}$ is the resonant multiplier for mean fields and $\mathcal{D}(\Omega) = \mathcal{D}|_{k=k_0+K}$ is the resonant multiplier for perturbation fields. Remember though that the measurable spectral density of stationary noise is the symmetrized one. For back-action noise it is evaluated from the symmetrized relation $2\pi\delta(\Omega - \Omega')\mathcal{S}_F(\Omega') = \frac{1}{2}\langle 0|F_{\text{BA}}(\Omega)F_{\text{BA}}^{\dagger}(\Omega') + F_{\text{BA}}^{\dagger}(\Omega)F_{\text{BA}}(\Omega')|0\rangle$, or explicitly $\mathcal{S}_F(\Omega) = \frac{1}{2}S_F(\Omega) + \frac{1}{2}S_F(-\Omega)$. However, the unsymmetrized spectral density makes a useful calculational tool, since in addition to its symmetric part being the measurable spectral density of back-action noise, its antisymmetric part is proportional to the introduced optical damping (see Sec. V). It also possesses certain heuristic value, in particular, giving an insight into the phenomenon of quantum noise interference. In this regard we refer also to the considerations presented in Ref. [48] on the interpretation of noise measurements of the ground-state cooling experiment [23].

The factors $\mathfrak{L}$ and $\mathfrak{D}$ in Eq. (10) describe contributions of vacuum noises from laser (a_{L}) and detector ports (a_{D}) respectively. Note that the contribution of a_{D} vanishes in the case of 100% reflective SR mirror, which is the case considered in Ref. [46]: a_{L} enters the interferometer and, if the latter is slightly offset from dark fringe, a small portion of a_{L} is transmitted into the SR port and gets enhanced in the effective cavity. Therefore, the field on the membrane surface is the sum of *two* fields, one that directly entered the interferometer from the input port and a second one which is given by the intracavity field. The former contribution is white shot noise while the latter one is the white noise Lorentz-filtered by the cavity, such that their interference leads to an asymmetric Fano-like profile in the shape of $S_F(\Omega)$, as described in Ref. [41]. Indeed, the frequency-dependent factor $\mathfrak{L}(\Omega)$ in Eq. (10) distorts the Lorentz-type denominator $\mathcal{D}(\Omega)$ creating an asymmetric profile with a characteristic dip at a particular frequency Ω_{Fano} where $S_F(\Omega_{\text{Fano}}) = 0$, being the result of *negative* interference between input and intracavity fields, see Fig. 3a. In cavity optomechanics this is identified with the emergence of dissipative coupling
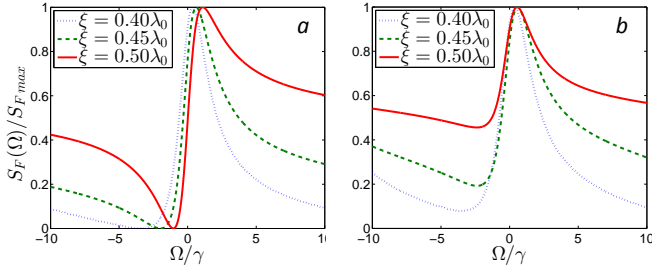
FIG. 3: Normalized (non-symmetrized) spectral densities of back-action noise for different membrane positions, $\xi = \delta l - \delta l_{DP}$ and δl_{DP} is defined by Eq. (3). For better visualization we choose membrane power reflectivity $R_m^2 = 0.3$, beamsplitter asymmetry $\delta_{BS} = -0.3$ and detuning $\Delta = 0$. a: $R_{SR}^2 = 1$. b: $R_{SR}^2 = 0.7$.

[41, 45, 46]

The expression for Ω_{Fano} is derived from the equation for $|\mathfrak{L}(\Omega)|^2 = 0$. In a narrow-band and low-frequency approximation one finds $\mathfrak{L}(\Omega) \approx 2(\alpha_1 + \Re\tilde{\alpha}_2) + 2i\Omega\frac{\mathcal{L}}{c}(\alpha_1 + \Re\tilde{\alpha}_2 + i\Im\tilde{\alpha}_2) + 2i\Delta\frac{\mathcal{L}}{c}2i\Im\tilde{\alpha}_2$, where $\tilde{\alpha}_2 = \alpha_2 e^{-i\arg\rho_2}$ and $\Delta = c\Delta_k$ is the detuning in frequency. In the particular regime of pure dissipative coupling the constant term (corresponding to dispersive coupling) vanishes, $\alpha_1 + \Re\tilde{\alpha}_2 = 0$, such that $\mathfrak{L}(\Omega_{\mathrm{Fano}}) = 0$ if $\Omega_{\mathrm{Fano}} = -2\Delta$, in agreement with Ref. [41].

Note also that if the interferometer with perfectly symmetric beamsplitter is tuned to dark port, the contribution of vacuum noise from the laser port in the back-action spectral density vanishes. This happens because counter-propagating beams in two arms are perfectly correlated so that the radiation pressure fluctuations caused by them cancel each other.

In a realistic interferometer, the SR mirror is not 100% reflective, therefore a_D enters the interferometer and gets resonantly enhanced. One would expect that its contribution to back-action noise has the form of a Lorentz factor, since there is no white vacuum noise from detector port to interfere with. Indeed, the factor $\mathfrak{D}$ is frequency-independent, such that the frequency dependence of the a_D contribution is solely defined by a Lorentz-type denominator $\mathcal{D}(\Omega)$, corresponding to pure dispersive coupling in an effective cavity. Therefore, in the back-action spectral density, the Lorentz-like summand adds to the Fano-like summand, leading to the blurring of characteristic features of Fano curve as illustrated in Fig. 3b. Vacuum noise from detector port no longer allows $S_F(\Omega)$ reaching zero, although the dip near Ω_{Fano} is still present. In an interferometer with symmetric beamsplitter and tuned to dark port, the contribution of vacuum noise from laser port cancels out, leaving only a pure Lorentzian back-action of vacuum noise from detector port.

V. DYNAMIC BACK-ACTION

Consider now a movable membrane with position operator $x_m(t)$ with a corresponding Fourier-transformed operator $x_m(\Omega)$. According to perturbation theory the fields on the membrane surfaces will have contributions of zeroth and first order in the mechanical displacement. One finds $\boldsymbol{B}_{m0} = \mathbb{M}_m \boldsymbol{A}_{m0}$ and $\boldsymbol{b}_m = \mathbb{M}_m \boldsymbol{a}_m + 2ik_0 x_m R_m \boldsymbol{A}_{m0}$. Thus the perturbation fields now contain both optical noises and the displacement of the membrane. Since the treatment of mean fields remains unchanged, we consider only the perturbation terms. The ingoing fields on the beamsplitter are defined by the equation $\boldsymbol{a}_{BS} = \mathbb{P}_R\mathbb{T}_R\boldsymbol{a}_{in} + \mathbb{P}_R\mathbb{R}_R\mathbb{P}_R\mathbb{M}_{MS}\boldsymbol{a}_{BS} + \mathbb{P}_R\mathbb{R}_R\mathbb{P}_R\mathbb{M}_{BS}^T\mathbb{P}_L\mathbb{P}_l\, 2ik_0 x_m(\Omega)R_m\boldsymbol{A}_{m0}$, with solution $\boldsymbol{a}_{BS} = \mathbb{K}_{MSR}\mathbb{P}_R\mathbb{T}_R\boldsymbol{a}_{in} + 2ik_0 x_m\mathbb{K}_{MSR}\mathbb{P}_R\mathbb{R}_R\mathbb{P}_R\mathbb{M}_{BS}^T\mathbb{P}_L\mathbb{P}_l R_m\boldsymbol{A}_{m0}$. Thus the incident and reflected fields on the membrane surfaces are

$$\boldsymbol{a}_m = \mathbb{M}_a\boldsymbol{a}_{in} + 2ik_0 x_m\mathbb{M}_{ax}\boldsymbol{A}_{m0}, \quad (11a)$$
$$\boldsymbol{b}_m = \mathbb{M}_b\boldsymbol{a}_{in} + 2ik_0 x_m(R_m\mathbb{I} + \mathbb{M}_m\mathbb{M}_{ax})\boldsymbol{A}_{m0}. \quad (11b)$$

The components of the relevant matrix

$$\mathbb{M}_{ax} = \mathbb{P}_l\mathbb{P}_L\mathbb{M}_{BS}\mathbb{K}_{MSR}\mathbb{P}_R\mathbb{R}_R\mathbb{P}_R\mathbb{M}_{BS}^T\mathbb{P}_L\mathbb{P}_l R_m.$$

are presented in the Appendix.

Substituting mean fields from Eqs. (8a, 8b) and perturbations fields (11a, 11b) into Eq. (9), ignoring the D.C. part and linearizing with respect to perturbation terms, one ends up with $F(\Omega) = F_{BA}(\Omega) + F_x(\Omega)$. Here F_{BA} is the radiation pressure noise considered in Sec. IV, and $F_x(\Omega) = -\mathcal{K}(\Omega)x_m(\Omega)$ is the ponderomotive force, i.e. dynamical part of the radiation pressure force caused by the motion of the membrane. The coefficient $\mathcal{K}(\Omega)$ modifies the dynamics of the membrane, and therefore represents the dynamic back-action,

$$\mathcal{K}(\Omega) = \frac{2ik_0}{c} R_m P_{in}\left[\mathbb{K}_{(1,1)}(\Omega) - \mathbb{K}_{(1,1)}^*(-\Omega)\right], \quad (12)$$
$$\mathbb{K}(\Omega) = \mathbb{M}_{B_0}^{*T}[\sigma_3 - 2\mathbb{M}_{ax}(\Omega)]\mathbb{M}_{A_0},$$

with $\sigma_3 = \mathrm{diag}(1, -1)$. If one denotes $K(\Omega) \equiv \Re[\mathcal{K}(\Omega)]$ and $\Gamma(\Omega) \equiv -\frac{1}{2}\Im[\mathcal{K}(\Omega)]/\Omega$, then the corresponding shifts of the square of intrinsic mechanical frequency and damping rate are equal to K/m and Γ/m [57].

The explicit formula for $\mathcal{K}(\Omega)$ is rather involved in the general case. We therefore present it using the following simplifying assumptions: (i) balanced beamsplitter, $\delta_{BS} = 0$, (ii) small displacements $\langle\delta x\rangle$ of the membrane from the position corresponding to dark fringe, $\langle\delta x\rangle = \xi/2$, $\xi = \delta l - \delta l_{DP}$, $\delta l_{DP} = n\lambda_0/4$, n is odd, $k_0\xi \ll 1$, and (iii) single optical mode with narrow linewidth, $\gamma\mathcal{L}/c \ll 1$. We also introduce the notations (cf. Eqs. (6, 7)),

$$\gamma = \gamma_{SR} + \gamma_m, \quad \gamma_{SR} = \frac{cT_{SR}^2}{4\mathcal{L}}, \quad \gamma_m = \frac{cR_m^2(k_0\xi)^2}{4\mathcal{L}},$$

$$\Delta = \delta_{\mathrm{SR}} + \delta_{\mathrm{m}}, \ \delta_{\mathrm{SR}} = \omega_0 - \omega_{\mathrm{c}}, \ \delta_{\mathrm{m}} = \pm \frac{cR_{\mathrm{m}}T_{\mathrm{m}}(k_0\xi)^2}{4\mathcal{L}}.$$

Here ω_{c} is the cavity resonance of interest in dark port regime, and the sign of δ_{m} alternates in the sequence of dark ports, starting with '+' for $n = 1$ (we assume that amplitude reflectivity and transmissivity are always positive). Note that both shifts in linewidth (γ_{m}) and detuning (δ_{m}) due to offset from dark fringe are *quadratic in displacement*. Under these assumptions Eq. (12) greatly simplifies to

$$\mathcal{K}(\Omega) = \frac{4\omega_0 R_{\mathrm{m}}^2 P_{\mathrm{in}}}{c\mathcal{L}} \frac{1}{\Delta^2 + (\gamma - i\Omega)^2}$$
$$\times \left\{ \frac{\delta_{\mathrm{SR}}[\gamma^2 + \Delta^2 - 4(\gamma\gamma_{\mathrm{m}} + \Delta\delta_{\mathrm{m}})]}{\gamma^2 + \Delta^2} \right.$$
$$\left. + \frac{2i(\gamma_{\mathrm{SR}}\delta_{\mathrm{m}} + \gamma_{\mathrm{m}}\delta_{\mathrm{SR}})\Omega + \delta_{\mathrm{m}}\Omega^2}{\gamma^2 + \Delta^2} \right\}. \quad (13)$$

This dynamic back-action possesses rich properties due to the complicated dependence on Δ and Ω. For $\xi = 0$ (on dark port) Eq. (13) reduces to Eqs. (1a, 1b). Off dark port for $\xi \neq 0$ typical plots of the 'anomalous' optical rigidity $K = K(\Delta)$ and damping $\Gamma = \Gamma(\Delta)$ are illustrated in Fig. 2c,d. One immediately notices that $\mathcal{K}(\Omega)|_{\Delta=0} \neq 0$ in general case. For optical damping this means that cooling of the membrane on resonance is possible. Several crossings of zero imply the appearance of additional regions of stability/instability on either side of the resonance. Note that using the fluctuation-dissipation theorem, one can reproduce the curves for $\Gamma = \Gamma(\Delta; \omega_{\mathrm{m}})$ at fixed mechanical frequency ω_{m}, from unsymmetrized back-action spectral density (10): since the emission/absorbtion rates of field quanta by the mechanical oscillator are defined by $S_F(\pm\omega_{\mathrm{m}})$, optical damping is proportional to their difference, $\Gamma \sim S_F(\omega_{\mathrm{m}}) - S_F(-\omega_{\mathrm{m}})$, i.e. to the antisymmetric part of spectral density [2].

Remember that in the effective-cavity approach, the transformation of the 'canonical' Lorentzian profile of S_F into the mixture of Lorentz- and Fano-like ones is governed by the interplay between dispersive and dissipative couplings in the cavity. Therefore, one can argue that the same mechanism leads to the transformation of 'canonical' dynamic back-action into the 'anomalous' one. Dynamic back-action corresponding to the pure dissipative coupling was considered in Ref. [45] in the context of cavity optomechanics. It was shown that although both optical spring and damping still remain antisymmetric with respect to Δ (and vanish at $\Delta = 0$), damping acquires additional regions of stability/instability.

Consider now a 100% reflective membrane in the MS interferometer. This is equivalent to a pure Michelson interferometer and, specifically, reproduces basic topology of the GW detectors where the differential motion of the end mirrors correspond to the motion of the membrane in the MS interferometer. Therefore the case of a quasi free mass, $\Omega \to 0$, is of particular interest. In this limit

Eq. (13) reduces to

$$K = \frac{4\omega_0 P_{\mathrm{in}}}{c\mathcal{L}} \frac{\Delta}{\gamma^2 + \Delta^2} \left[1 - \frac{4\gamma\gamma_{\mathrm{m}}}{\gamma^2 + \Delta^2} \right], \quad (14a)$$

$$\Gamma = -\frac{4\omega_0 P_{\mathrm{in}}}{c\mathcal{L}} \frac{\gamma\Delta}{(\gamma^2 + \Delta^2)^2} \left[1 - \frac{\gamma_{\mathrm{m}}}{\gamma} \frac{3\gamma^2 - \Delta^2}{\gamma^2 + \Delta^2} \right]. \quad (14b)$$

Both K and Γ vanish on resonance, and one can check using Eq. (13) that this feature holds for any Ω. Terms in square brackets in Eqs. (14a, 14b) represent the deviations from 'canonical' formulas. According to them, optical spring can have three zeroes at $\Delta = 0$ and $\Delta = \pm\sqrt{\gamma(4\gamma_{\mathrm{m}} - \gamma)}$, if $\gamma_{\mathrm{m}} > \gamma/4$. Remember that the 'canonical' spring (1a) only has one zero for small Ω. Similarly, the optical damping can also cross zero three times at $\Delta = 0$ and $\Delta = \pm\gamma\sqrt{(3\gamma_{\mathrm{m}} - \gamma)/(\gamma + \gamma_{\mathrm{m}})}$, if $\gamma_{\mathrm{m}} > \gamma/3$. Thus, for a large enough offset from dark fringe, one gets several intersecting regions of positive/negative K and Γ, as illustrated in Fig. 2b. This may have an impact on the operation of advanced GW detectors, since they will utilize the DC-readout scheme, when a small offset from dark fringe is created artificially to get some mean power for homodyning, thus resulting in 'anomalous' spring/damping, if $\Delta \neq 0$ and the offset from dark fringe ξ is large enough. This can raise certain control issues, in turn. For the 'anomalous' spring/damping to be manifest (at least at low frequencies), one can use the following rough estimation of the corresponding value of ξ: $\gamma_{\mathrm{m}} > \gamma_{\mathrm{SR}}/2$, or explicitly, $\xi/\lambda_0 > \sqrt{T_{\mathrm{SR}}^2/(8\pi^2)}$. Note, however, that the MS interferometer under consideration includes neither power-recycling technique, nor arm-cavities, therefore this estimation should be applied to realistic interferometers with certain reserve.

Accurate analysis of stability reveals that there exists a certain region of parameters where the set of K and Γ makes a stable configuration. This can be utilized for the reduction of quantum noise in the interferometric topologies, designed to overcome the standard quantum limit, that rely on the effect of optical spring (such as detuned SR-topologies, optical bars [49] and optical levers [49, 50]), since it becomes possible to sustain stable optical spring with only a single laser carrier, that is not possible with conventional optical spring.

VI. OBSERVATION OF ANOMALOUS, TWO-SIDED DYNAMICAL INSTABILITY

Our experimental setup was in direct analogy to Fig. 1. The Michelson-Sagnac interferometer [51] had an arm length of about 7.5 cm and contained a non-stoichiometric silicon nitride (SiN) membrane arranged such that its two transmitted and its two reflected beams overlapped with an interference contrast of greater 99.9%. The MS interferometer acted as a compound retro-reflector for light that entered either of its two ports. Its reflectivity was a function of the microscopic position of the membrane along the direction of the laser

beam. We controlled the membrane position via a piezo-electric element (piezo). A highly reflective cavity mirror ($R_{\mathrm{SR}}^2 = 99.97\,\%$) located in the signal output port, with a macroscopic distance of $1.2\,\mathrm{cm}$ to the beamsplitter, established a standing-wave signal-recycling cavity [52], whose second end mirror was defined by the MS interferometer. Similar to current gravitational wave detector arrangements, the light leaving this port was detected by a PIN photo diode. The experiment was carried out with laser light at a wavelength of $1064\,\mathrm{nm}$. The membrane's normal incidence power reflectivity at this wavelength was $R_{\mathrm{m}}^2 = 17\,\%$. The membrane had a thickness of $40\,\mathrm{nm}$, a side length of $1.5\,\mathrm{mm}$ and a resonance frequency of $133\,\mathrm{kHz}$ [53]. The interferometer was operated inside a vacuum chamber to avoid gas damping or acoustic excitation of the membrane motion. We determined the mechanical quality factor Q of the fundamental oscillation mode for different pressures. As result, we found $Q = 6 \cdot 10^5$ for gas pressures below $4 \cdot 10^{-6}\,\mathrm{mbar}$. A detailed description of the interferometer is given in Refs. [54, 55].

For all membrane positions our interferometric cavity arrangement operated outside the resolved sideband regime due to the membrane's low resonance frequency, the short cavity round trip length of $2 \cdot 8.7\,\mathrm{cm}$, and intracavity losses mainly caused by the imperfect beam splitter. The cavity thus resonantly enhanced the upper and lower signal sidebands produced by the membrane motion as well as the remaining dim carrier light in a broadband fashion.

In a first series of measurements we positioned the membrane such that the carrier light of all four beams reflected off and transmitted through the membrane showed a strong destructive interference in the interferometer's signal output port, i.e. established an almost dark port. We observed parametric cooling as well as heating as it is well-known for dispersive optomechanics. When the pump light was *blue* detuned with respect to the cavity resonance we observed strong heating of the mechanical motion. For a *red* detuned cavity we observed optical cooling as expected. In a second series of measurements we positioned the membrane such that about 1% of the input laser light was transmitted through the SR cavity, which corresponded to the maximal light transmission through the cavity arrangement possible. Fig. 4 shows the light power transmitted through the SR cavity when the position of the SR mirror was slowly scanned over cavity resonance. At the start of the scan the SR cavity was too long to resonate. When the optical resonance was approached, first, the dynamical instability occurred that is also present for operations close to the interferometer dark port. On cavity resonance the oscillations were rapidly damped indicating a region of stability. When the cavity was further shortened, not optical cooling but a second distinct instability occurred, as predicted for the anomalous dynamic back-action off dark port. As shown in the right part of Fig. 4 the amplitude of this instability was significantly smaller than that on
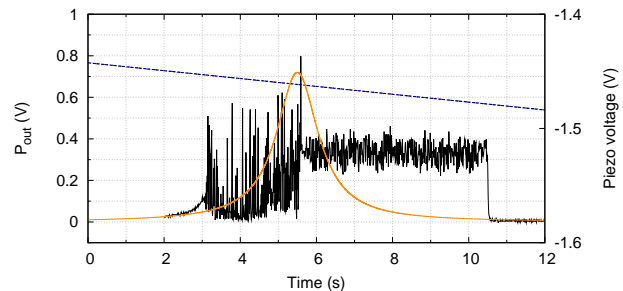

FIG. 4: Black: Time series of the Michelson Sagnac interferometer's output power P_{out} while linearly decreasing the signal recycling cavity length. The dashed blue line is a linear fit to the piezo voltage. For fast cavity length scans an undisturbed cavity resonance peak was found (solid orange line) since there was not sufficient time for the instabilities to build up. For slow scanning speeds, as given by the x-axis labeling, instabilities on both sides of the resonance were observed. Both resonances were dynamical, i.e. one or more frequencies were attributed to them. When the detuning crosses zero (resonant case), the oscillations were damped indicating a regime of stability.

the left branch.

VII. SUMMARY AND CONCLUSION

In this paper we theoretically and experimentally analyzed the optomechanics of a signal-recycled Michelson-Sagnac interferometer containing a semitransparent membrane. In contrast to previous works we did not restrict our consideration to the dark port regime of operation but rather considered a general situation corresponding to the arbitrary position of the membrane. Such an interferometer can be equivalently described as an effective Fabry-Perot cavity with one of the mirrors having a reflectivity that depends on the position of the membrane. Mechanical motion of the latter modulates resonance frequencies *and linewidth* of the effective cavity, featuring the so-called dispersive and dissipative couplings. In particular, unsymmetrized spectral density of back-action noise exhibits the mixture of Lorentz- and Fano-like resonances, the latter owned to the interference of input and intracavity laser fields on the membrane.

We then proceeded with the study of dynamic back-action effects, optical spring and optical damping. We found that in the interferometer operated off dark port, these effects behave differently from the conventional ones: both spring and damping become highly asymmetric with respect to detuning and acquire non-zero values at zero detuning. This, in principle, allows cooling of the membrane on resonance. Additionally, optical damping acquires several regions of stability and instability.

We presented experimental data that indeed proves the existence of two regions of instability for a membrane

Michelson-Sagnac interferometer operated off dark port. The instabilities were observed for red as well as for blue detuned laser light. Both instabilities were dynamical and showed quantitative differences in their oscillation amplitudes. A detailed quantitative characterization of both instability regions is in progress.

In the extreme case of a 100% reflecting membrane, corresponding to the well-studied pure Michelson interferometer, dynamic back-action vanishes on resonance independently of the dark-port offset, but demonstrates 'anomalous' features when operated off-resonance and off dark-port: both optical spring and damping exhibit several intersecting regions of positive/negative values (for a large enough offset). For a certain region of parameters this allows, in particular, maintaining the stable set of optical spring and damping with only a single laser carrier in a free-mass interferometer. Moreover, advanced gravitational-wave detectors with DC-readout that are currently under construction, can also encounter anomalous optical spring off-resonance (given large enough offset from the dark fringe), raising certain control issues.

Our analysis thus demonstrates that the interferometers operated *off dark port* violate the scaling law in the sense that the latter one only covers the equivalence between a Fabry-Perot cavity and the interferometers operated *at dark port*. This opens new possibilities for designing the interferometer topologies aimed at reduction of quantum noise and overcoming the standard quantum limit in gravitational-wave detectors. On the other hand, in cavity optomechanics these effects may turn helpful for finding new regimes of cavity-assisted cooling.

Acknowledgments

Appendix A: Useful matrices

Matrix $\mathbb{M}_A$:

$$\mathbb{M}_A^{(1,1)} = \mathcal{D}^{-1}\Big[T_{\mathrm{BS}}\left(1 - R_{\mathrm{m}}R_{\mathrm{SR}}e^{2ik(\mathcal{L}+\delta l/2)}\right)$$
$$+ R_{\mathrm{BS}}T_{\mathrm{m}}R_{\mathrm{SR}}e^{2ik\mathcal{L}}\Big]e^{ik(L+l-\delta l/2)},$$
$$\mathbb{M}_A^{(1,2)} = -\mathcal{D}^{-1}T_{\mathrm{SR}}R_{\mathrm{BS}}e^{ik(\mathcal{L}-\delta l/2)},$$
$$\mathbb{M}_A^{(2,1)} = \mathcal{D}^{-1}\Big[R_{\mathrm{BS}}\left(1 + R_{\mathrm{m}}R_{\mathrm{SR}}e^{2ik(\mathcal{L}-\delta l/2)}\right)$$
$$+ T_{\mathrm{BS}}T_{\mathrm{m}}R_{\mathrm{SR}}e^{2ik\mathcal{L}}\Big]e^{ik(L+l+\delta l/2)},$$
$$\mathbb{M}_A^{(2,2)} = \mathcal{D}^{-1}T_{\mathrm{SR}}T_{\mathrm{BS}}e^{ik(\mathcal{L}+\delta l/2)}.$$

Matrix $\mathbb{M}_B$:

$$\mathbb{M}_B^{(1,1)} = \mathcal{D}^{-1}\Big[-T_{\mathrm{BS}}\left(R_{\mathrm{m}} - R_{\mathrm{SR}}e^{2ik(\mathcal{L}+\delta l/2)}\right)$$
$$+ T_{\mathrm{m}}R_{\mathrm{BS}}e^{ik\delta l}\Big]e^{ik(L+l-\delta l/2)},$$
$$\mathbb{M}_B^{(1,2)} = \mathcal{D}^{-1}T_{\mathrm{SR}}\left(R_{\mathrm{BS}}R_{\mathrm{m}} + T_{\mathrm{m}}T_{\mathrm{BS}}e^{ik\delta l}\right)e^{ik(\mathcal{L}-\delta l/2)},$$
$$\mathbb{M}_B^{(2,1)} = \mathcal{D}^{-1}\Big[R_{\mathrm{BS}}\left(R_{\mathrm{m}} + R_{\mathrm{SR}}e^{2ik(\mathcal{L}-\delta l/2)}\right)$$
$$+ T_{\mathrm{m}}T_{\mathrm{BS}}e^{-ik\delta l}\Big]e^{ik(L+l+\delta l/2)},$$
$$\mathbb{M}_B^{(2,2)} = \mathcal{D}^{-1}T_{\mathrm{SR}}\left(T_{\mathrm{BS}}R_{\mathrm{m}} - T_{\mathrm{m}}R_{\mathrm{BS}}e^{-ik\delta l}\right)e^{ik(\mathcal{L}+\delta l/2)}.$$

Matrix $\mathbb{M}_{ax}$:

$$\mathbb{M}_{ax}^{(1,1)} = \mathcal{D}^{-1}R_{\mathrm{m}}R_{\mathrm{BS}}^2 R_{\mathrm{SR}}e^{2ik(\mathcal{L}-\delta l/2)},$$
$$\mathbb{M}_{ax}^{(2,2)} = \mathcal{D}^{-1}R_{\mathrm{m}}T_{\mathrm{BS}}^2 R_{\mathrm{SR}}e^{2ik(\mathcal{L}+\delta l/2)},$$
$$\mathbb{M}_{ax}^{(1,2)} = \mathbb{M}_{ax}^{(2,1)} = -\mathcal{D}^{-1}R_{\mathrm{m}}R_{\mathrm{BS}}T_{\mathrm{BS}}R_{\mathrm{SR}}e^{2ik\mathcal{L}}.$$

[1] V. B. Braginsky and F. Ya. Khalili, *Quantum Measurement* (Cambridge University Press, Cambridge, 1992).
[2] A. A. Clerk, M. H. Devoret, S. M. Girvin, F. Marquardt, R. J. Schoelkopf, Rev. Mod. Phys. **82**, 1155 (2010), arXiv:0810.4729v2 [cond-mat.mes-hall].
[3] S. L. Danilishin, F. Ya. Khalili, Liv. Rev. Rel. **15**, 5 (2012), URL http://http://relativity.livingreviews.org/Articles/lrr-2012-5.
[4] V. B. Braginsky, Sov. Phys. JETP **26**, 831 (1968).
[5] V. B. Braginsky and Yu. I. Vorontsov, Sov. Phys. Usp. **17**, 644 (1975).
[6] V. B. Braginsky, Yu. I. Vorontsov and F. Ya. Khalili, Sov. Phys. JETP **46**, 705 (1977).
[7] T. P. Purdy, R. W. Peterson, C. A. Regal, to be published (2012), arXiv:1209.6334 [quant-ph].
[8] V. B. Braginsky, A. B. Manukin, Sov. Phys. JETP **25**, 653 (1967).
[9] V. B. Braginsky, A. B. Manukin, M. Yu. Tikhonov, Sov. Phys. JETP **31**, 829 (1970).
[10] T. Corbitt, D. Ottaway, E. Innerhofer, J. Pelc, N. Mavalvala, Phys. Rev. A **74**, 021802(R) (2006), arXiv:gr-qc/0511022.
[11] I. Wilson-Rae, N. Nooshi, W. Zwerger, T. J. Kippenberg, Phys. Rev. Lett. **99**, 093901 (2007), arXiv:cond-mat/0702113 [cond-mat.mes-hall].
[12] F. Marquardt, J. P. Chen, A. A. Clerk, S. M. Girvin, Phys. Rev. Lett. **99**, 093902 (2007), arXiv:cond-mat/0701416 [cond-mat.mes-hall].
[13] O. Arcizet, P.-F. Cohadon, T. Briant, M. Pinard and A. Heidmann, Nature **444**, 71 (2006).
[14] P. F. Cohadon, A. Heidmann and M. Pinard, Phys. Rev. Lett. **83**, 3174 (1999).

[15] S. Gigan, H. R. Bhm, M. Paternostro, F. Blaser, G. Langer, J. B. Hertzberg, K. C. Schwab, D. Buerle, M. Aspelmeyer and A. Zeilinger, Nature **444**, 67 (2006).

[16] S. Grblacher, J. B. Hertzberg, M. R. Vanner, G. D. Cole, S. Gigan, K. C. Schwab and M. Aspelmeyer, Nature Physics **5**, 485 (2009).

[17] C. H. Metzger, K. Karrai, Nature **432**, 1002 (2004).

[18] C. A. Regal, J. D. Teufel and K. W. Lehnert, Nature Physics **4**, 555 (2008).

[19] R. Rivire, S. Delglise, S. Weis, E. Gavartin, O. Arcizet, A. Schliesser and T. J. Kippenberg, Phys. Rev. A **83**, 063835 (2011).

[20] T. Rocheleau, T. Ndukum, C. Macklin, J. B. Hertzberg, A. A. Clerk and K. C. Schwab, Nature **463**, 72 (2010).

[21] J. D. Thompson, B. M. Zwickl, A. M. Jayich, F. Marquardt, S. M. Girvin, J. G. E. Harris, Nature **452**, 72 (2008).

[22] J. D. Teufel *et al.*, Nature **475**, 359 (2011).

[23] J. Chan *et al.*, Nature **478**, 89 (2011).

[24] V. B. Braginsky, M. L. Gorodetsky, F. Ya. Khalili, Phys. Lett. A **232**, 340 (1997).

[25] F. Ya. Khalili, Phys. Lett. A **288**, 251 (2001), arXiv:gr-qc/0107084.

[26] M. Rakhmanov, Ph.D. thesis, California Institute of Technology (2000), URL `http://www.ligo.caltech.edu/docs/P/P000002-00.pdf`.

[27] A. Buonanno, Y. Chen, Phys. Rev. D **65**, 042001 (2002), arXiv:gr-qc/0107021.

[28] A. Buonanno, Y. Chen, Phys. Rev. D **67**, 062002 (2003), arXiv:gr-qc/0208048.

[29] V. I. Lazebny, S. P. Vyatchanin, Phys. Lett. A **344**, 7 (2005).

[30] F. Ya. Khalili, V. I. Lazebny, S. P. Vyatchanin, Phys. Rev. D **73**, 062002 (2006), arXiv:gr-qc/0511008.

[31] `www.advancedligo.mit.edu`.

[32] H. Rehbein, H. Mueller-Ebhardt, K. Somiya, S. L. Danilishin, R. Schnabel, K. Danzmann, Y. Chen, Phys. Rev. D **78**, 062003 (2008), arXiv:0805.3096 [gr-qc].

[33] T. Corbitt, Y. Chen, H. Mueller-Ebhardt, E. Innerhofer, D. Ottaway, H. Rehbein, D. Sigg, S. Whitcomb, C. Wipf, N. Mavalvala, Phys. Rev. Lett. **98**, 150802 (2007), arXiv:quant-ph/0612188v2.

[34] A. Rakhubovsky, S. Hild, S. Vyatchanin, Phys. Rev. D **84**, 062002 (2011), arXiv:1102.4266 [gr-qc].

[35] A. Rakhubovsky, S. Vyatchanin, Phys. Lett. A **376**, 1405 (2012), arXiv:1201.6196 [gr-qc].

[36] F. Khalili, S. Danilishin, H. Mueller-Ebhardt, H. Miao, Y. Chen, C. Zhao, Phys. Rev. D **83**, 062003 (2011), arXiv:1010.1124 [gr-qc].

[37] G. M. Harry (for the LIGO Scientic Collaboration), Class. Quantum Grav. **27**, 084006 (2010).

[38] LIGO Scientific Collaboration, LIGO document T1200199 (2012), URL `https://dcc.ligo.org/public/0091/T1200199/002/wp2012.pdf`.

[39] R. Adhikari, K. Arai, S. Ballmer, E. Gustafson, S. Hild, LIGO document T1200031 (2012).

[40] ET Science Team, ET-0106C-10 (2011), URL `https://tds.ego-gw.it/itf/tds/file.php?callFile=ET-0106C-10.pdf`.

[41] F. Elste, S. M. Girvin, A. A. Clerk, Phys. Rev. Lett. **102**, 207209 (2009), arXiv:0903.2242v2 [cond-mat.mes-hall].

[42] M. Li, W. H. P. Pernice and H. X. Tang, Phys. Rev. Lett. **103**, 223901 (2009).

[43] S. Huang and G. S. Agarwal, Phys. Rev. A **82**, 033811 (2010).

[44] S. Huang and G. S. Agarwal, Phys. Rev. A **81**, 053810 (2010).

[45] T. Weiss, C. Bruder, A. Nunnenkamp, to be published (2012), arXiv:1211.7029 [quant-ph].

[46] A. Xuereb, R. Schnabel, K. Hammerer, Phys. Rev. Lett. **107**, 213604 (2011), arXiv:1107.4908 [physics.optics].

[47] B. Willke *et al.*, Class. Quantum Grav. **23**, S207 (2006).

[48] F. Ya. Khalili, H. Miao, H. Yang, A. H. Safavi-Naeini, O. Painter, Y. Chen, to be published (2012), arXiv:1206.0793 [quant-ph].

[49] F. Ya. Khalili, Phys. Lett. A **317**, 169 (2003), arXiv:gr-qc/0304060v1.

[50] S. L. Danilishin, F. Ya. Khalili, Phys. Rev. D **73**, 022002 (2006), arXiv:gr-qc/0508022v1.

[51] K. Yamamoto, D. Friedrich, T. Westphal, S. Goßler, K. Danzmann, K. Somiya, S. L. Danilishin, R. Schnabel, Rev. Rev. A **81**, 33849 (2010), arXiv:0912.2603v2 [quant-ph].

[52] B. J. Meers, Phys. Rev. D **38**, 2317 (1988).

[53] H. Kaufer, A. Sawadsky, T. Westphal, D. Friedrich, R. Schnabel, New J. Phys. **14**, 095018 (2012), arXiv:1205.2241 [quant-ph].

[54] D. Friedrich, H. Kaufer, T. Westphal, K. Yamamoto, A. Sawadsky, F. Y. Khalili, S. Danilishin, S. Goßler, K. Danzmann, R. Schnabel, New J. Phys. **13**, 93017 (2011), arXiv:1104.3251 [physics.optics].

[55] T. Westphal, D. Friedrich, H. Kaufer, K. Yamamoto, S. Goßler, H. Müller-Ebhardt, S. L. Danilishin, F. Ya. Khalili, K. Danzmann, and R. Schnabel, LSC review (2011).

[56] For other choices of transfer matrices (2) the dark port condition will correspond to a different δl but this is insignificant, since the absolute phase does not matter

[57] Assuming that the equation of motion of the membrane is of the following form: $\ddot{x} + 2\gamma_{\mathrm{m}}\dot{x} + \omega_{\mathrm{m}}^2 x = F(t)/m$.